Frontiers of Information Technology & Electronic Engineering
www.zju.edu.cn/jzus; engineering.cae.cn; www.springerlink.com
ISSN 2095-9184 (print); ISSN 2095-9230 (online)
E-mail: jzus@zju.edu.cn

Level-direction decomposition analysis with a focus on image watermarking framework*

M. F. KAZEMI[1], M. A. POURMINA[1], A. H. MAZINAN[‡2]

([1]*Department of Electrical and Computer Engineering, Science and Research Branch, Islamic Azad University, Tehran, Iran*)

([2]*Department of Control Engineering, Faculty of Electrical Engineering, South Tehran Branch, Islamic Azad University, Tehran, Iran*)

E-mail: mfkazemi@srbiau.ac.ir; pourmina@srbiau.ac.ir; mazinan@azad.ac.ir

Received May 20, 2015; Revision accepted Feb. 16, 2016; Crosschecked Oct. 17, 2016

Abstract: This research addresses the new level-direction decomposition in the area of image watermarking as the further development of investigations. The main process of realizing a watermarking framework is to generate a watermarked image with a focus on contourlet embedding representation. The approach performance is evaluated through several indices including the peak signal-to-noise ratio and structural similarity, whereby a set of attacks are carried out using a module of simulated attacks. The obtained information is analyzed through a set of images, using different color models, to enable the calculation of normal correlation. The module of the inverse of contourlet embedding representation is correspondingly employed to obtain the present watermarked image, as long as a number of original images are applied to a scrambling module, to represent the information in disorder. This allows us to evaluate the performance of the proposed approach by analyzing a complicated system, where a decision making system is designed to find the best level and the corresponding direction regarding contourlet embedding representation. The results are illustrated in appropriate level-direction decomposition. The key contribution lies in using a new integration of a set of subsystems, employed based upon the novel mechanism in contourlet embedding representation, in association with the decision making system. The presented approach is efficient compared with state-of-the-art approaches, under a number of serious attacks. A number of benchmarks are obtained and considered along with the proposed framework outcomes. The results support our ideas.

Key words: Level-direction decomposition analysis, Watermarking framework, Contourlet embedding representation, Scrambling module, Simulated attacks

http://dx.doi.org/10.1631/FITEE.1500165 **CLC number:** TP391.41

1 Introduction

Various investigations in the area of image watermarking have been carried out with respect to state-of-the-art approaches. The outcomes have suggested a number of efficient solutions, due to the fact that traditional outcomes may be improved in both real and academic environments. With this goal, our present research is to make a new contribution in the field of image watermarking through contourlet embedding (CT) representation. The primary process of the image watermarking framework is organized in the present investigation using level-direction decomposition transformation to generate watermarked images, while the module of the inverse of CT embedding representation (ICT) is obtained to retrieve the watermarked images. In the same way, the scrambling module is obtained to represent the information in disorder for a number of original images that can be applied to the proposed framework. This allows us to evaluate the performance of the proposed approach by analyzing a complicated system, where a decision making system is designed to find the best level and the corresponding direction for CT embedding representation in the process of level-direction

‡ Corresponding author

* Project supported by the Islamic Azad University, Iran

ORCID: M. F. KAZEMI, http://orcid.org/0000-0001-6557-9437; A. H. MAZINAN, http://orcid.org/0000-0002-8810-9574

© Zhejiang University and Springer-Verlag Berlin Heidelberg 2016

decomposition. The peak signal-to-noise ratio (PSNR) and structural similarity (SSIM) indices are employed to evaluate the approach performance, as long as a number of attacks via the module of simulated attacks are included in the proposed framework to enable the calculation of normal correlation (NC).

Prior to presenting the proposed framework, we review the related research in the area. Regarding watermark research, Niu *et al.* (2011) suggested a color image watermarking scheme in the non-sampled CT embedding representation domain. The geometrically invariant space was first realized through color image normalization, while a region was acquired from the normalized color image via invariant centroid theory. Following that, the non-sampled CT embedding representation transform was performed on the green channel of the same region. The digital watermark was embedded into the host color image by amending the low frequency non-sampled CT embedding representation transform coefficients, in which masking can be used to control the strength of watermark embedding.

Ali *et al.* (2015) presented an image watermarking algorithm in the wavelet domain, under optimized compensation of singular value decomposition, using artificial bee colony. They proposed a robust image watermarking algorithm, developed in the wavelet domain based on singular value decomposition and artificial bee colony. Shao *et al.* (2015) suggested an approach for combining double random phase encoding in color image watermarking with its application in a quaternion gyrator domain, by addressing a joint encryption-watermarking system with more security in association with double random phase encoding applicable in the present domain. Zhan *et al.* (2014) considered a blind watermarking approach to be applicable in three-dimensional mesh models along with a vertex curvature. In this embedding approach, the local window of the vertex is used to calculate the root mean square curvature for every vertex of the 3D mesh model, while an ordered set of fluctuation values is acquired. Moreover, the algorithm uses a blind watermark extraction technique to extract the watermark information. Chen and Zhu (2012) proposed a robust watermarking approach through a combination of QR factorization and discrete cosine transform. The blocks with small modifications were chosen as the embedding locations. This minimizes the embedding distortion to improve the imperceptibility of the approach.

Yadav *et al.* (2015) proposed a phase-image watermarking scheme in a gyrator domain using Devil's vortex Fresnel lens, taken as a phase mask, by providing much-desired parameter-rich phase masks which contribute to the enhanced security while overcoming the axis alignment problem in optical setup. Qi *et al.* (2015) explained image watermarking using polar harmonic transform. There was a polar linear canonical transform in line with the linear canonical transform to improve the traditional results on the security of watermarking information. Ali and Ahn (2015) commented on an optimized gray-scale image watermarking through a firefly algorithm, using discrete wavelet transform (DWT) and singular value decomposition (SVD) schemes. They validated the objective of this method that cannot be used for protection of rightful ownership. Ouyang *et al.* (2015) investigated color image watermarking in association with quaternion Fourier transform and the improved uniform log-polar mapping. Note that the outcome embeds dual watermarks, one first taken as a meaningful binary image watermark and the other then taken as a bipolar watermark.

Dinh *et al.* (2014) realized real-time 3D human pose recovery from a single depth image through principal direction analysis. Both quantitative and qualitative evaluations were made in the 3D human pose recovering methodology. Agarwal *et al.* (2015) discussed a gray-scale image watermarking through hybrid fuzzy-based architecture, where watermarks extracted yield high normalized correlation values, indicating a successful watermark recovery. Dadkhah *et al.* (2014) presented an effective SVD-based image tampering detection and self-recovery through active watermarking by generating two distinct tamper detection keys based on SVD regarding the image blocks. Guo and Prasetyo (2014) introduced false-positive-free SVD based image watermarking. The present watermarking was realized by embedding the principal component of a watermark into the host image in the block based manner through the spread spectrum concept.

Abdallah *et al.* (2014) presented image watermarking under SVD in the reflectance component after applying the transform. There is a block-by-block implementation to make the watermark more

robust to attacks. Tsougenis *et al.* (2014) presented adaptive color image watermarking through quaternion image moments to exploit rotation invariance, reconstruction capability, and computation accuracy subject to the tradeoff between robustness and imperceptibility. Yu *et al.* (2015) suggested a fragile watermarking method in stereo image authentication under localization and recovery. A detection technique using a part of the alterable-length watermark is realized to increase the accuracy of tamper localization. Mishra *et al.* (2014) proposed a gray-scale image watermarking. The singular values of a binary watermark were all embedded into singular values regarding the sub-band coefficients related to the host image by using multiple scaling factors. Makbol and Khoo (2014) focused on a robust and secure digital image watermarking scheme, while integer wavelet transform and SVD were realized that can be used for copyright protection.

Al-Otum (2014) investigated semi-fragile watermarking for grayscale image authentication and tamper detection in association with an adjusted expanded-bit multi-scale quantization based technique. The results are based on implementing a modified DWT quantization based algorithm, embedding a random watermark bit sequence into the present transformation. Lei *et al.* (2014) proposed a reversible watermarking scheme in the area of medical image processing in line with differential evolution. Signature information and textual data were inserted into the original medical images along with a recursive dither modulation algorithm, where wavelet transform and SVD were realized. Chen *et al.* (2014) suggested a full quaternion discrete Fourier transform (QDFT) in association with watermarking in color images. This approach is to establish the links that exist between the discrete Fourier transform (DFT) regarding the three RGB color channels and the corresponding components regarding the QDFT coefficients, as long as a general unit pure quaternion is considered. Do *et al*. (2001) presented pyramidal directional filter banks and curvelets as well.

Consider the other potential investigations in this area in concise forms. Cai *et al.* (2015) presented a difference angle quantization index modulation scheme in image watermarking, while Wang XY *et al.* (2014) proposed a robust color image watermarking through local quaternion exponent moments. Yang *et al.* (2014) explained a geometric correction based robust color image watermarking scheme using quaternion exponent moments, while Tao *et al.* (2014) reviewed robust image watermarking in transform domains and geometric invariant regions. Wang H *et al.* (2014) proposed an image restoration approach in line with structured side information with its application to image watermarking. Tsougenis *et al.* (2013) discussed the adaption of image watermarking in the polar harmonic transform domain. Agarwal *et al.* (2013) investigated gray scale image watermarking through the hybrid network of the genetic algorithm and back propagation neural networks (GA-BPN), while Su *et al.* (2014) proposed a color image blind watermarking scheme in line with QR decomposition.

Compared with the above reviewed studies, the contribution of this study can be summarized as follows: (1) The integration of the set of elements employed in the proposed watermarking framework including the scrambling module, decision making, level-direction decomposition, CT embedding representation, simulated attacks, ICT, and PSNR-SSIM-NC (PSN) is novel; (2) A new mechanism in CT embedding representation is illustrated to generate watermarked images with respect to various state-of-the-art approaches; (3) A decision making system is designed to find the best level and the corresponding direction in the CT embedding representation during level-direction decomposition; (4) The approach performance is evaluated through the calculation of a number of indices, while some attacks via the module of simulated attacks are carried out in a set of image colored models, indicating that the approach presented here is coherently efficient.

2 The proposed watermarking framework

The proposed watermarking framework is as illustrated in Fig. 1. To discuss the proposed framework, in a brief form, note that the original image has to be applied to the scrambling module to organize the present image in disorder. We need to use a complicated system to evaluate the performance of the proposed approach. A decision making module is used to find the best level and the corresponding direction regarding CT embedding representation, in which its results are illustrated in the level-direction

decomposition module. The main process of the watermarking framework is designed under the proposed idea via CT embedding to generate watermarked images. The module of ICT is correspondingly realized to retrieve the present watermarked image. It is the right time to consider the approach performance through calculations of PSNR and SSIM, which are discussed in the proceeding sections, while a number of attacks via the simulated attack module are carried out in the output of ICT to enable the calculation of NC, integrated in the PSN module.

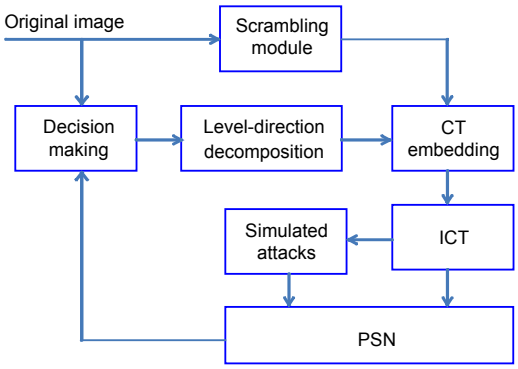

Fig. 1 The proposed watermarking framework

2.1 Scrambling module

There are a number of methods to scramble the logo images, e.g., the pseudo random number sequence and the Arnold transform. The Arnold transform is acting in the 2D representation, i.e., A: $T^2 \rightarrow T^2$. Note that the input and the corresponding output dimensionality regarding the present transform are the same, as given by

$$\begin{bmatrix} x' \\ y' \end{bmatrix} = \begin{bmatrix} 2 & 1 \\ 1 & 1 \end{bmatrix} \begin{bmatrix} x \\ y \end{bmatrix} \bmod N, \tag{1}$$

where N is taken as the log image size and $x, y \in \{0, 1, \ldots, N-1\}$. Note that one of the important specifications regarding the present transform is known as the periodic one.

2.2 CT embedding representation

The idea of realizing CT embedding representation is based on the pyramid directional filter bank (PDFB), as briefly illustrated in Fig. 2. Fig. 2a presents the structure of dividing the frequencies with respect to their angles used in the output of Fig. 2b, to describe the main structure of PDFB, which uses high- and low-pass filters along with the down sampler module. Fig. 3 illustrates how to calculate the pyramid of the image. The image input at the Jth level is first fed to the present block, where the approximation information at the $(J-1)$th level and the corresponding prediction information at the Jth level are acquired.

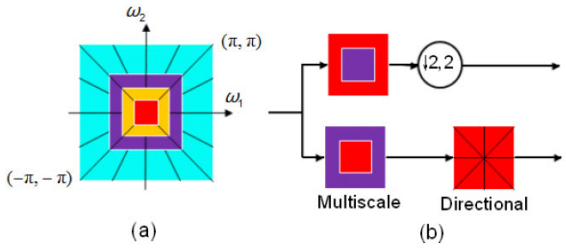

Fig. 2 Schematic of the pyramid directional filter bank (PDFB): (a) dividing the frequencies with respect to their angles; (b) the main structure

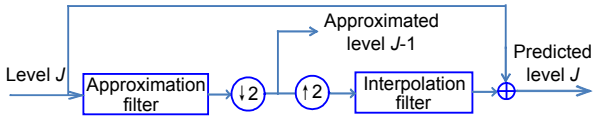

Fig. 3 Schematic of pyramid-level calculations

With a focus on the analysis and synthesis of filter banks, the Laplacian pyramid (LP) scheme is shown in Fig. 4.

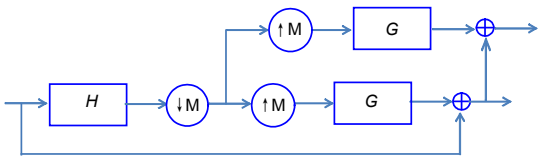

Fig. 4 Laplacian pyramid scheme

Note that the present mechanism is iterated to reach the 0th level (Fig. 5). Considering CT embedding representation, it is organized based on LP and the directional filter bank (DFB) for a 512×512 image (Fig. 6). This was first proposed by Do and Vetterli (2001) to represent contours and their textures regarding the image in an efficient manner. CT embedding representation is organized by a double filter bank structure to obtain sparse expansions for typical images under smooth contours, as long as LP is first realized to capture the point discontinuities.

Afterwards, a directional filter bank is obtained to link point discontinuities to its linear structures.

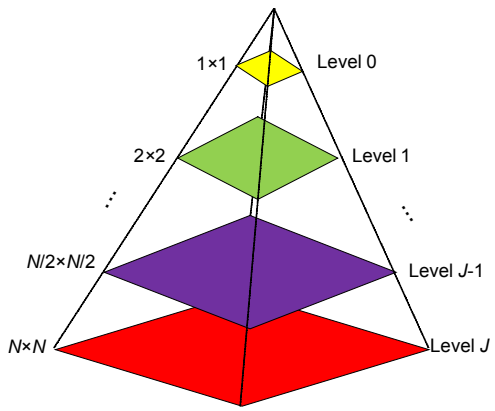

Fig. 5 Schematic of the iterated pyramid levels regarding the input image

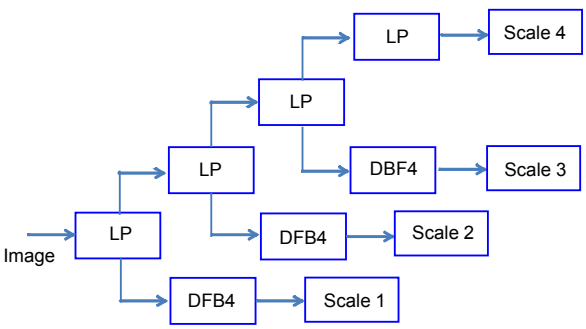

Fig. 6 CT embedding representation through LP and DFB (Ali and Ahn, 2015)

Also, note that the overall outcomes regarding CT embedding representation are presented as an image expansion via basic elements such as contour segments. The high frequency sub-band images are fed from LP to DFB to capture the direction information. It is obvious that by CT embedding representation the image is decomposed into directional sub-bands at multiple scales, which can smoothly iterate the low frequency sub-band image.

2.3 CT embedding mechanism

CT embedding mechanism is realized based upon the watermarking intensities, taken as α. This is working to insert the logo information via Eq. (2) by choosing the level and its direction through the intelligent decision making system in the process of CT embedding representation:

$$I_{\mathrm{WL,D}}(i,j)=I_{\mathrm{L,D}}(i,j)[1+\alpha w(n)], \tag{2}$$

where $I_{\mathrm{L,D}}(i, j)$ indicates the sub-bands regarding the CT embedding representation in the pyramid level and the direction, and $I_{\mathrm{WL,D}}(i, j)$ indicates the watermarked image. In the approach proposed here, CT embedding representation coefficients in the form of a tree including parent-child are to be modified in a number of levels and the corresponding directions (Fig. 7).

In the present approach, the elements of the tree to be embedded are simply indexed by L_{ij}, where i and j indicate its level and direction regarding the present tree, respectively. The second level can be used if the coefficients regarding L_{21} and L_{22} need to be updated. In this example, the coefficients of L_{21} and L_{22} are taken as the parent node, and the coefficients of L_{12} and L_{14} are taken as the child node. Note that the present tree has five coefficients, one located in L_{22} and the rest in the children nodes (two related to L_{12} and two related to L_{14}). Now, the embedding mechanism will be implemented in the following procedure. The host gray scale image is first chosen in the size of $M\times M$ pixels and the binary logo titled W is then chosen in the size of $M_W\times N_W$ pixels.

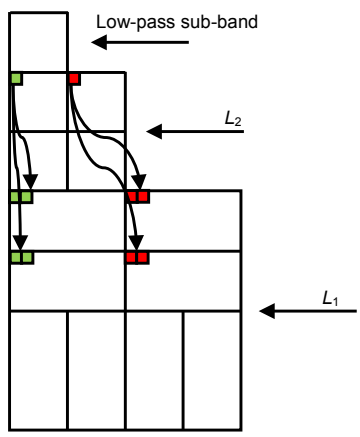

Fig. 7 CT embedding representation coefficients tree

Step 1: The binary logo W is presented in a sequence of −1 and 1 as

$$w^*=\{w_k^*\,|\,k=1,2,\ldots,M_W\times N_W;w_k^*=-1,1\}. \tag{3}$$

Step 2: After applying CT embedding representation to the original image and determining the corresponding coefficients, the aforementioned tree is organized. Based upon the relationship between the parent and child for each coefficient in the sub-band,

four equaled coefficients are chosen, two of them related to one pyramid level and the rest related to the same level.

Step 3: Calculate the maximum and the minimum for the child node of the tree.

Step 4: The coefficients of the sub-band of the child node are varied to be embedded as

$$\text{value_of_root_node}(i,j) = \begin{cases} \text{maximum value of child node} + \alpha, & w_k^* = 1, \\ \text{minimum value of child node} - \alpha, & w_k^* = -1, \end{cases} \quad (4)$$

where w_k^* is taken as the kth bit regarding the logo and α the watermarking intensity.

Step 5: By applying ICT to the watermarked image, the original image with the logo is retrieved.

The procedure of retrieving the logo from the processed host image is implemented without knowing the original image or parameter α:

Step 1: By applying CT embedding representation to the final results obtained in the previous procedure, the image with the logo is analyzed for the level and the corresponding direction.

Step 2: Based upon the coefficients in the sub-band, the suitable tree can now be chosen. As parameter α is not available, at this point of time, an appropriate threshold has to be determined. One idea is to calculate the average value of the four coefficients of the child.

Step 3: The bits regarding the logo are calculated by

$$w_e = \begin{cases} 1, & \text{Value_of_root_node} \geq \text{Mean}^*, \\ -1, & \text{Value_of_root_node} < \text{Mean}^*. \end{cases} \quad (5)$$

Step 4: The sequence of information in step 3 is reorganized in the form of an image:

$$W_e = M_W \times N_W \text{ pixels.} \quad (6)$$

2.4 Level-direction decomposition

Consider the level-direction regarding CT embedding representation based upon the size of the logo such as 32×32 or 64×64. In one such case, as presented in Fig. 8, the levels can be taken as 2, 3, or 4 and the corresponding direction as 1, 2, 3, or 4. It is obvious that 24 and 20 states are acquired with the logo sizes of 32×32 and 64×64, respectively.

2.5 PSN module

The PSN module is organized based upon the calculations of PSNR, SSIM, and NC, respectively. It is obtained through an integration of the aforementioned modules by considering the output results with respect to the corresponding input images. In fact, the present module allows us to consider the approach performance accurately and efficiently. Based upon the results, the approach performance verification can be presented in a better form with respect to other related ones. PSNR is denoted as

$$\text{PSNR} = 10 \cdot \log \frac{M \times N \times 255^2}{\sum_{m=0}^{M-1} \sum_{n=0}^{N-1} \left[I_O(m,n) - I_W(m,n) \right]^2}, \quad (7)$$

where the size of the images I_O and I_W are taken as $M \times N$.

SSIM is presented as

$$\text{SSIM}(x,y) = \frac{2\mu_x \mu_y + C_1}{\mu_x^2 + \mu_y^2 + C_1} \frac{2\delta_{xy} + C_2}{\delta_x^2 + \delta_y^2 + C_2}, \quad (8)$$

where δ_x and δ_y are first taken as the standard deviations regarding the samples of x and y. Also, δ_{xy} is taken as the cross correlation, and μ_x and μ_y are taken as the corresponding averaged values. The parameters C_1 and C_2 are then taken as constant values. Finally the NC for the x and y images is written as

$$\text{NC} = \frac{\sum_{m=0}^{M-1} \sum_{n=0}^{N-1} x(m,n) \cdot y(m,n)}{\sum_{m=0}^{M-1} \sum_{n=0}^{N-1} x(m,n)^2}, \quad (9)$$

where the image sizes are taken as $M \times N$ as well.

2.6 Decision making module

The decision making module is used to decide the type of cover image and the corresponding logo image as well as the levels and corresponding directions of the decompositions to be watermarked, for considering the approach performance in a comparable manner.

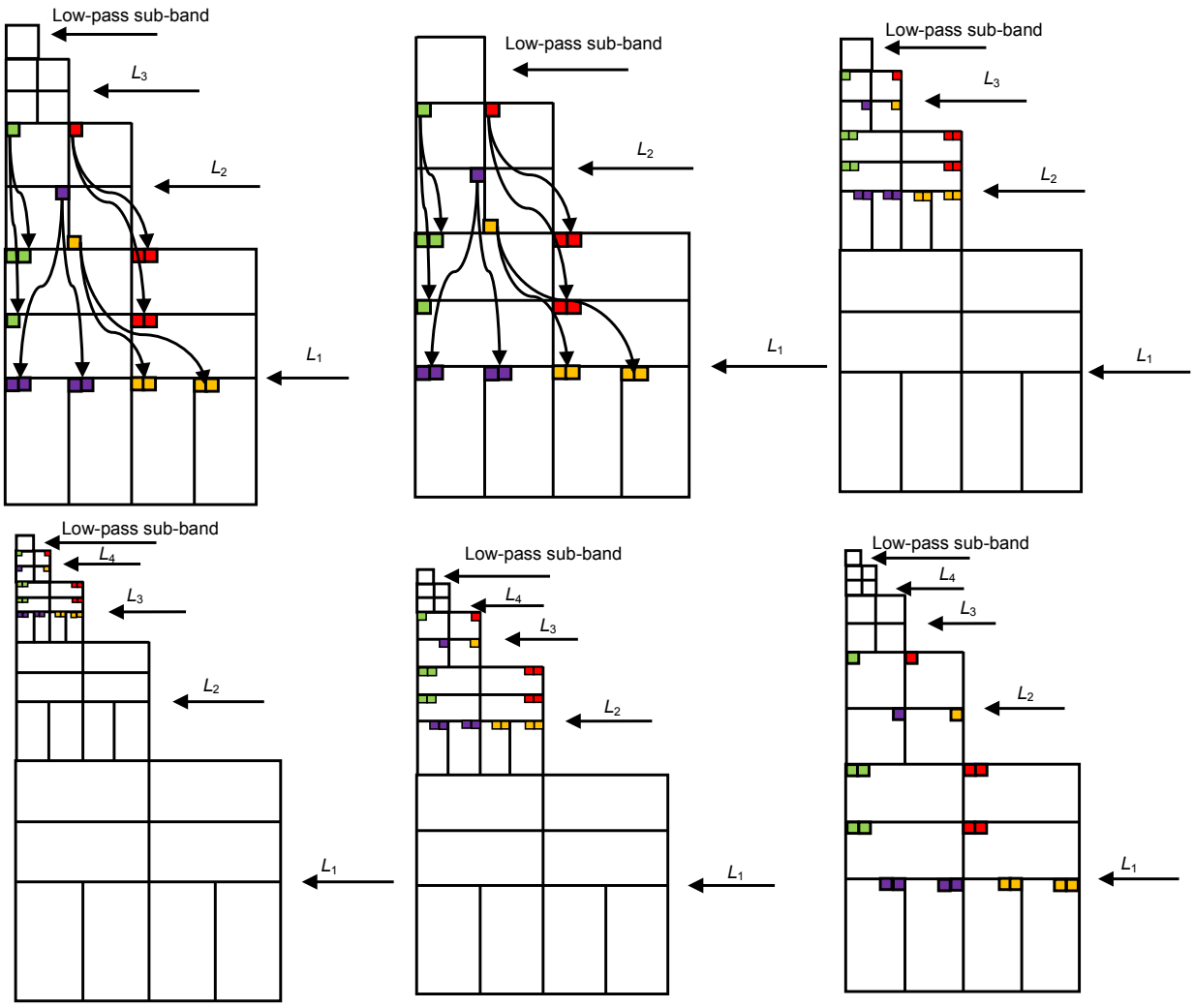

Fig. 8 The levels and the corresponding directions regarding CT embedding representation

2.7 Simulated attacks

There are a number of intentional and unintentional attacks: (1) JPEG compressions in the separate qualities from 10% to 90%, (2) Gaussian noise, impulse noise, and Salt & Pepper noise, (3) median filter in separate sizes, (4) averaged filter in separate sizes, and crops in separate sizes, and (5) rotations in separate angles in both clockwise and anti-clockwise directions and finally scaling in separate values.

3 Experimental results

The Arnold was used in the experiment as the original logo image. It can be retrieved after a number of transformations. To explain further, the following standard information, as illustrated in Fig. 9, was processed via the Arnold algorithm. In this experiment, the algorithm was carried out P=300 times. The results indicated that in the 300th iteration the original image was retrieved accurately. A number of cover images along with the logo image used in the experiments are illustrated in Fig. 10. The experimental results are organized, while the information regarding optimization is also used.

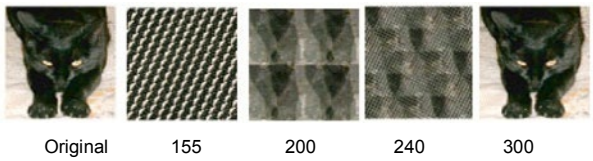

Fig. 9 An image processed via the Arnold algorithm
In the 300th iteration the original image was retrieved accurately

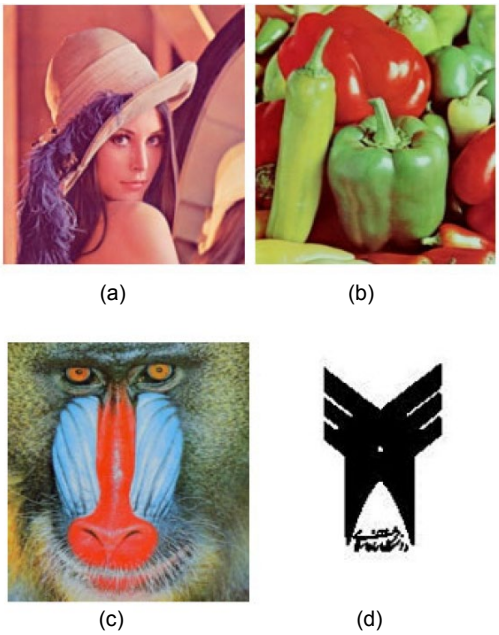

Fig. 10 A number of cover images (a–c) and the logo image (d) used in the experiments

The cover images used include Lena, Peppers, and Baboon in the size of 512×512 and the logo images in the size of 32×32.

CT embedding representation results regarding the Lena image are illustrated in Fig. 11. Lena was chosen as the cover image and the size of the logo image was set as 32×32, to be used in the process of watermarking. This is obtained for different levels regarding CT embedding representation, in which some of the watermark intensity values against JPEG compression attacks through the calculation of NC are illustrated in Fig. 12.

The proposed approach is considered once more, against a number of separate crop attacks. The investigated outcomes are tabulated in Table 1.

Table 2 shows the results regarding the watermarking using the 32×32 logo image through SSIM and PSNR in the three images, for different levels and directions under a set of intensity values. Eq. (10) is proposed to evaluate the set of experiments under 38 different attacks.

Note that Eq. (10) is organized to assign an overall score to the set of experimental results based on the outcomes along with NC. As the proposed approach has been carried out in a number of separate situations, including 'no attack', 'JPEG compressions', 'cropping', 'filtering', and 'scaling', the

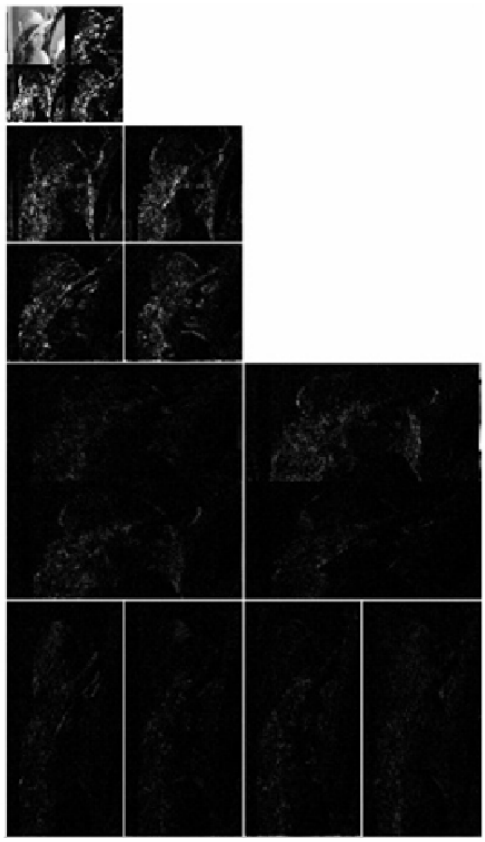

Fig. 11 CT embedding representation results regarding the Lena image

$$\begin{aligned}\text{Score} = {} & \text{NC}_{\text{No attack}} \cdot \frac{1}{9}\sum_{Q=10\%}^{90\%} \text{NC}_{\text{JPEG}(Q)} + \frac{\text{PSNR}}{38} + 2\text{SSIM} \\ & + \frac{1}{6}\sum_{i=1}^{6} \text{NC}_{\text{Filtering}(i)} + \frac{1}{9}\sum_{i=1}^{9} \text{NC}_{\text{Noise}(i)} + \frac{1}{7}\sum_{i=1}^{7} \text{NC}_{\text{Cropping}(i)} \\ & + \frac{1}{2}\sum_{i=1}^{2} \text{NC}_{\text{Scaling}(i)} + \frac{1}{4}\sum_{i=1}^{4} \text{NC}_{\text{Rotation}(i)} \\ & + \text{NC}_{\text{Histogram equalization}}.\end{aligned} \tag{10}$$

results regarding the whole of the attacks need to be first acquired. Then, the average values are documented to present an assessment criterion. In fact, Eq. (10) presents the average results of the whole of the experiments, while each of the investigated outputs is considered to present the approach performance and its verification. Table 2 shows the finalized results regarding the watermarking through the calculation of Eq. (10) in the three separate images in different levels and directions under a set of intensity values. The notations LS, DL, LE, and Dn are taken

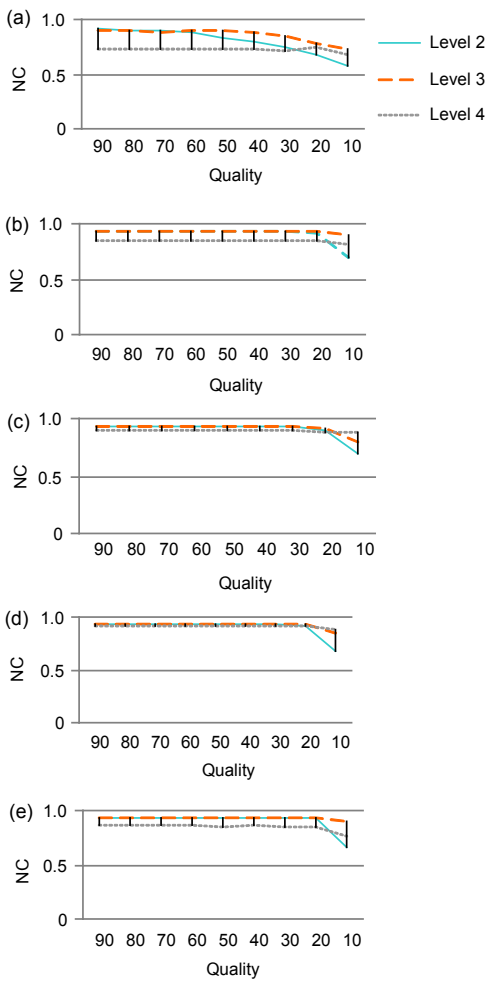

Fig. 12 The results regarding NC in the Lena image against a number of compression attacks in the four levels under a set of intensity values
(a) Direction 1, α=10; (b) Direction 1, α=50; (c) Direction 2, α=50; (d) Direction 3, α=50; (e) Direction 4, α=50

as the logo size, decomposition level, level embedding, and direction, respectively, and the corresponding integration information is related to the indices. Table 3 shows the results of the watermarking by calculating the score in the three images. The outcomes are acquired in different levels and directions under a set of intensity values.

An attempt is made to consider the applicability of the proposed approach in different color models. To compare the results in a reasonable manner, the intensity of the watermarking of the referenced channel of the color models can be presented in the new channel by

$$\alpha_{\mathrm{n}} = \frac{\alpha_{\mathrm{ref}} R_{\text{n-channel}}}{R_{\text{ref-channel}}}, \tag{11}$$

where α_{ref} is taken as the referenced intensity of the watermarking that is related to the referenced channel and α_{n} is taken as the new intensity of the watermarking. Moreover, $R_{\text{n-channel}}$ indicates the difference of the maximum intensity and the corresponding minimum intensity in the new channel of the color models, and $R_{\text{ref-channel}}$ represents the same definition in the referenced channel of the color model.

It is obvious that different color models lead to different outcomes. Therefore, the optimum solutions need to be verified.

A series of experiments using the color models can be carried out to indicate the performances of the proposed approach, reflected based upon PSNR, SSIM, and NC, as long as a number of cover images

Table 1 The results regarding NC in the Lena image against a number of crop attacks in four directions under a set of intensity values

Crop attack	NC								
	α=10			α=50			α=90		
	Level 2	Level 3	Level 4	Level 2	Level 3	Level 4	Level 2	Level 3	Level 4
Crop 1, 6%	0.8796	0.8722	0.6701	0.8990	0.8990	0.7845	0.9123	0.9019	0.8113
Crop 2, 6%	0.9153	0.899	0.7132	0.9227	0.9227	0.8321	0.9227	0.9272	0.8663
Crop 3, 6%	0.8871	0.8826	0.7028	0.8960	0.9049	0.8009	0.9034	0.9153	0.8321
Crop 4, 6%	0.8960	0.8752	0.6835	0.9049	0.9004	0.8068	0.9094	0.9034	0.8455
Crop 5, 25%	0.8960	0.8752	0.6835	0.9049	0.9004	0.8068	0.9094	0.9034	0.8455
Crop 6, 12.5%	0.8796	0.8722	0.6909	0.8915	0.9004	0.8068	0.8990	0.9108	0.8425
Crop 7, 12.5%	0.8722	0.8796	0.7147	0.8826	0.9004	0.8262	0.8900	0.9227	0.8529

Table 2 The results for watermarking through SSIM and PSNR in the three separate images in different levels and directions under a set of intensity values

Index	Lena						Index	Peppers					
	α=10		α=50		α=90			α=10		α=50		α=90	
	SSIM	PSNR	SSIM	PSNR	SSIM	PSNR		SSIM	PSNR	SSIM	PSNR	SSIM	PSNR
32221	99	44.62	96	37.96	92	33.84	32221	99	46.96	97	38.68	92	34.24
32222	99	44.60	96	36.25	90	32.56	32222	99	47.04	96	37.61	90	33.01
32223	99	46.27	96	37.81	91	33.38	32223	99	47.07	96	38.15	91	33.61
32224	99	46.80	97	39.09	93	34.79	32224	99	47.09	97	39.30	93	34.95
32321	99	44.62	96	37.96	92	33.84	32321	99	46.96	97	38.68	92	34.24
32322	99	44.60	96	36.25	90	32.56	32322	99	47.04	96	37.61	90	33.01
32323	99	46.27	96	37.81	91	33.38	32323	99	47.07	96	38.15	91	33.61
32324	99	46.80	97	39.09	93	34.79	32324	99	47.09	97	39.30	93	34.95
32331	97	36.90	93	34.45	87	31.83	32331	98	38.71	94	35.67	87	32.61
32332	97	37.54	92	33.91	83	30.74	32332	98	39.15	92	34.86	83	31.34
32333	98	40.61	93	35.88	86	32.27	32333	98	39.85	93	35.70	85	32.25
32334	98	41.81	95	37.61	90	34.13	32334	98	39.46	94	36.48	89	33.55
32421	99	44.62	96	37.96	92	33.84	32421	99	46.96	97	38.68	92	34.24
32422	99	44.60	96	36.25	90	32.56	32422	99	47.04	96	37.61	90	33.01
32423	99	46.27	96	37.81	91	33.38	32423	99	47.07	96	38.15	91	33.61
32424	99	46.80	97	39.09	93	34.79	32424	99	47.09	97	39.30	93	34.95
32431	97	36.90	93	34.45	87	31.83	32431	98	38.71	94	35.67	87	32.61
32432	97	37.54	92	33.91	83	30.74	32432	98	39.15	92	34.86	83	31.34
32433	98	40.61	93	35.88	86	32.27	32433	98	39.85	93	35.70	85	32.25
32434	98	41.81	95	37.61	90	34.13	32434	98	39.46	94	36.48	89	33.55
32441	88	29.24	85	28.52	80	27.59	32441	89	29.86	85	29.12	80	28.15
32442	87	28.80	80	27.24	71	25.65	32442	87	29.10	80	27.75	72	26.22
32443	93	32.90	88	30.87	81	28.76	32443	91	31.64	86	30.10	79	28.33
32444	95	34.86	94	34.03	92	32.94	32444	92	31.76	91	31.37	88	30.77

Index	Baboon						Index	Baboon					
	α=10		α=50		α=90			α=10		α=50		α=90	
	SSIM	PSNR	SSIM	PSNR	SSIM	PSNR		SSIM	PSNR	SSIM	PSNR	SSIM	PSNR
32221	99	42.28	98	37.39	96	33.63	32421	99	42.28	98	37.39	96	33.63
32222	99	42.74	99	36.60	95	32.52	32422	99	42.74	99	36.60	95	32.52
32223	99	41.75	98	36.66	96	32.87	32423	99	41.75	98	36.66	96	32.87
32224	99	41.09	98	37.25	96	33.92	32424	99	41.09	98	37.25	96	33.92
32321	99	42.28	98	37.39	96	33.63	32431	98	36.35	96	33.56	92	31.02
32322	99	42.74	99	36.60	95	32.52	32432	98	36.35	95	32.85	90	29.94
32323	99	41.75	98	36.66	96	32.87	32433	97	35.66	95	32.80	91	30.26
32324	99	41.09	98	37.25	96	33.92	32434	97	35.79	96	33.60	93	31.45
32331	98	36.35	96	33.56	92	31.02	32441	94	30.98	92	29.86	89	28.57
32332	98	36.35	95	32.85	90	29.94	32442	94	30.74	90	28.58	84	26.58
32333	97	35.66	95	32.80	91	30.26	32443	95	31.18	91	29.25	87	27.40
32334	97	35.79	96	33.60	93	31.45	32444	96	31.15	95	30.58	94	29.90

Table 3 The results regarding watermarking through the calculation of the score in the three separate images in different levels and directions under a set of intensity values

Index	LS	DL	LE	Dn	Score								
					Lena			Peppers			Baboon		
					α=10	α=50	α=90	α=10	α=50	α=90	α=10	α=50	α=90
32221	32	2	2	1	9.5865	9.7588	9.6338	9.5765	9.7251	9.5958	9.1843	9.7009	9.6689
32222	32	2	2	2	9.5539	9.6735	9.5421	9.6495	9.7218	9.5663	9.2072	9.6719	9.6051
32223	32	2	2	3	9.6462	9.7523	9.6057	9.6636	9.7457	9.6097	9.2596	9.6809	9.6270
32224	32	2	2	4	9.7203	9.8051	9.6791	9.6702	9.7960	9.6613	9.3017	9.7045	9.6993
32321	32	3	2	1	9.5865	9.7588	9.6338	9.5765	9.7251	9.5958	9.1843	9.7009	9.6689
32322	32	3	2	2	9.5539	9.6735	9.5421	9.6495	9.7218	9.5663	9.2072	9.6719	9.6051
32323	32	3	2	3	9.6462	9.7523	9.6057	9.6636	9.7457	9.6097	9.2596	9.6809	9.6270
32324	32	3	2	4	9.7203	9.8051	9.6791	9.6702	9.7960	9.6613	9.3017	9.7045	9.6993
32331	32	3	3	1	9.4318	9.8659	9.7923	9.4885	9.9372	9.8290	9.5611	9.9205	9.8789
32332	32	3	3	2	9.1584	9.7280	9.6160	9.2995	9.7821	9.6667	9.4329	9.8529	9.7823
32333	32	3	3	3	9.4749	9.9133	9.7855	9.4436	9.8915	9.7575	9.4454	9.8886	9.8121
32334	32	3	3	4	9.9268	10.0881	9.9402	9.7547	10.0220	9.8970	9.7752	10.001	9.9440
32421	32	4	2	1	9.5865	9.7588	9.6338	9.5765	9.7251	9.5958	9.1843	9.7009	9.6689
32422	32	4	2	2	9.5539	9.6735	9.5421	9.6495	9.7218	9.5663	9.2072	9.6719	9.6051
32423	32	4	2	3	9.6462	9.7523	9.6057	9.6636	9.7457	9.6097	9.2596	9.6809	9.6270
32424	32	4	2	4	9.7203	9.8051	9.6791	9.6702	9.7960	9.6613	9.3017	9.7045	9.6993
32431	32	4	3	1	9.4318	9.8659	9.7923	9.4885	9.9372	9.8290	9.5611	9.9205	9.8789
32432	32	4	3	2	9.1584	9.7280	9.6160	9.2995	9.7821	9.6667	9.4329	9.8529	9.7823
32433	32	4	3	3	9.4749	9.9133	9.7855	9.4436	9.8915	9.7575	9.4454	9.8886	9.8121
32434	32	4	3	4	9.9268	10.0881	9.9402	9.7547	10.022	9.8970	9.7752	10.0010	9.9440
32441	32	4	4	1	8.1286	8.8653	9.1777	7.9284	8.9132	9.2379	8.8408	9.5201	9.6516
32442	32	4	4	2	8.7998	9.2398	9.2572	8.4932	9.2157	9.2734	9.2725	9.6583	9.6647
32443	32	4	4	3	9.1234	9.6825	9.6250	8.9316	9.5973	9.5749	9.4447	9.8010	9.7645
32444	32	4	4	4	8.5244	9.4386	9.6480	8.3297	9.1397	9.3686	8.8287	9.3551	9.5623

LS: logo size; DL: decomposition level; LE: level embedding; Dn: direction

are used to consider them in comparable manner. A variation of watermarking intensity in the span of 0–100 is considered, where a number of attacks are carried out to provide a challenging environment for the proposed approach to be judged. These results are important for evaluating the applicability of the approach in different color models. Note that the overall outcomes indicate that the proposed approach is able to extract the logo image from the corresponding cover image with desirable accuracy, while the performance of the cover image does not decrease in this process.

The results of the watermarking through PSNR, SSIM, NC, and the overall score are tabulated in Table 4 for the three separate images using different channels in the RGB model.

Note that the constant watermarking intensity in the whole of the experiments is taken as 50. Fig. 13 shows the results of the RGB model against the JPEG compression attacks through the calculation of NC.

The results of the watermarking through PSNR, SSIM, NC, and the overall score are tabulated in Table 5 for the three separate images for different channels in the YIQ model.

The results of the YIQ model are considered in the present cover images against the JPEG compression attacks through the calculation of NC (Fig. 14).

The results of the watermarking through PSNR, SSIM, NC, and the overall score in the three separate images for different channels in the YCbCr model are tabulated in Table 6.

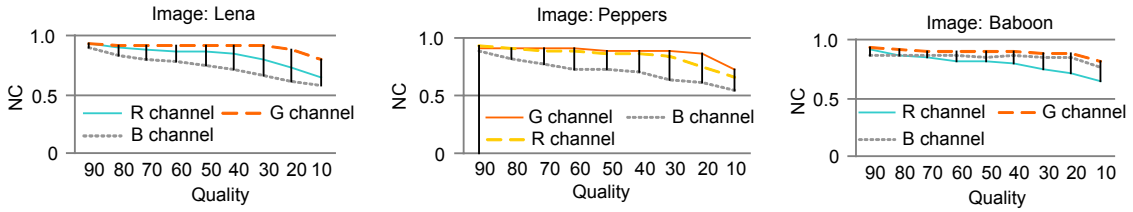

Fig. 13 Calculation of NC against JPEG compression attacks in the RGB model

Table 4 The results regarding the watermarking through SSIM and PSNR in the three separate images for different channels in the RGB model

Channel	PSNR			SSIM		
	Lena	Peppers	Baboon	Lena	Peppers	Baboon
R	37.96	37.20	33.71	0.9853	0.9830	0.9860
G	37.58	35.82	33.09	0.9863	0.9823	0.9866
B	38.05	37.05	32.86	0.9846	0.9841	0.9872
Channel	**Score**			**NC**		
	Lena	Peppers	Baboon	Lena	Peppers	Baboon
R	10.0483	10.0237	9.9378	0.9346	0.9346	0.9346
G	10.1117	10.0573	9.9942	0.9331	0.9346	0.9346
B	9.9754	9.9481	9.8438	0.9346	0.9346	0.9316

Table 5 The results regarding the watermarking through PSNR, SSIM, NC, and the overall score in the three separate images for different channels in the YIQ model

Channel	PSNR			SSIM		
	Lena	Peppers	Baboon	Lena	Peppers	Baboon
Y	38.58	37.10	33.95	0.9368	0.9550	0.9663
I	50.95	47.40	43.58	0.9958	0.9913	0.9920
Q	52.65	47.31	48.85	0.9975	0.9926	0.9981
Channel	**Score**			**NC**		
	Lena	Peppers	Baboon	Lena	Peppers	Baboon
Y	10.1118	10.0631	9.9968	0.9331	0.9346	0.9346
I	10.1613	10.2933	10.2130	0.9346	0.9346	0.9346
Q	10.1631	10.0904	10.2275	0.9346	0.9346	0.9346

Table 6 The results regarding watermarking through PSNR, SSIM, NC, and the overall score in the three separate images for different channels in the YCbCr model

Channel	PSNR			SSIM		
	Lena	Peppers	Baboon	Lena	Peppers	Baboon
Y	37.64	36.70	33.72	0.9547	0.9507	0.9646
Cb	48.16	48.45	46.05	0.9907	0.9931	0.9936
Cr	46.43	44.54	43.69	0.9905	0.9823	0.9900
Channel	**Score**			**NC**		
	Lena	Peppers	Baboon	Lena	Peppers	Baboon
Y	10.0980	10.0448	9.9943	0.9346	0.9346	0.9346
Cb	10.2089	10.1063	10.2552	0.9346	0.9346	0.9346
Cr	10.1973	10.2566	10.2669	0.9346	0.9346	0.9346

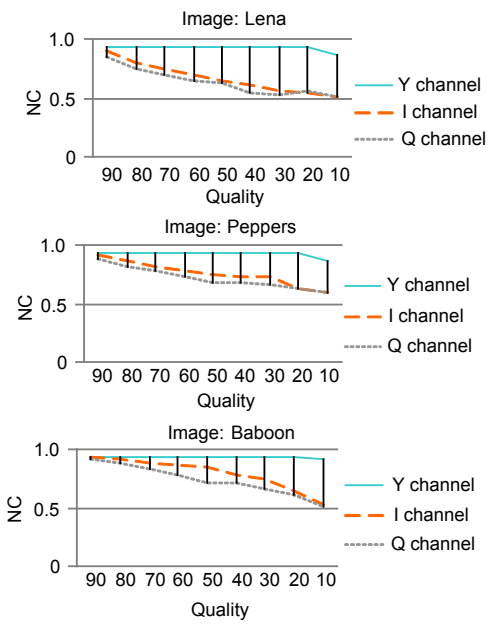

Fig. 14 Calculation of NC against JPEG compression attacks in the YIQ model

The results of the YCbCr model are considered in the present cover images against the JPEG compression attacks through the calculation of NC (Fig. 15).

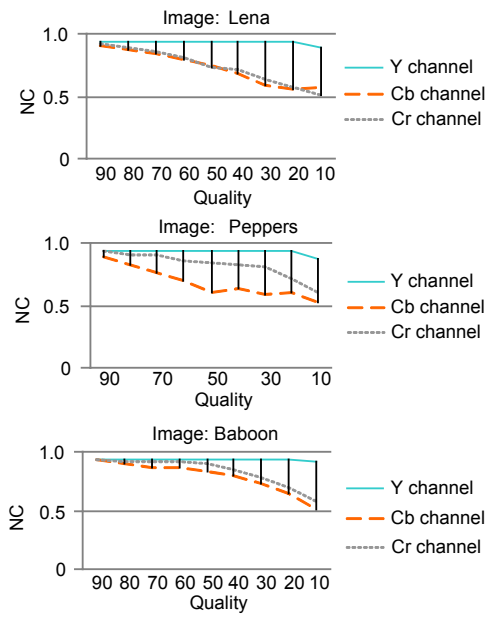

Fig. 15 Calculation of NC against JPEG compression attacks in the YCbCr model

The results of watermarking through PSNR, SSIM, NC, and the overall score in the three separate images for different channels in the HSI model are tabulated in Table 7.

The results of the HSI model are illustrated in the present cover images against the JPEG compression attacks through calculation of NC (Fig. 16).

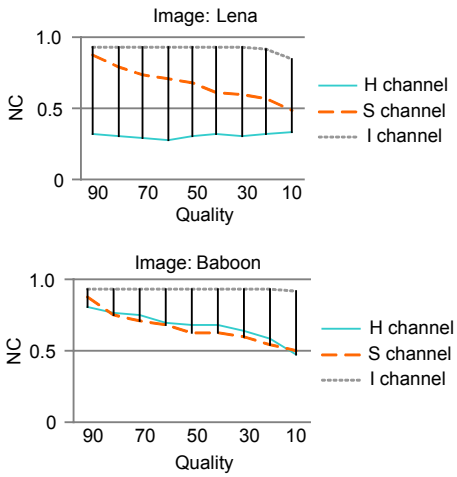

Fig. 16 Calculation of NC against JPEG compression attacks in the HSI model

The results of the watermarking through PSNR, SSIM, NC, and the overall score in the three separate images for different channels in the HSV model are tabulated in Table 8.

The results of the HSV model are given in the present cover images against the JPEG compression attacks through the calculation of NC (Fig. 17).

There are two assessment criteria, the first related to NC under the constant watermarking intensity with JPEG attacks and the second related to PSNR and SSIM under the first cover image. With a focus on the first assessment, the G channel of the RGB model, the Y channels of both YIQ and YCbCr models, the I channel of the HSI model, and finally the V channel of the HSV model all well behaved. In the present assessment, the Y channels of both YIQ and YCbCr and also the I channel of HSI have the best performance with respect to the other related channels. Moreover, with a focus on the second assessment, the B and G channels of RGB, the Q channel of YIQ, the Cb channel of YCbCr, and the S channels of both HSV and HSI all well behaved. Note that the Q channel of YIQ has the best performance with respect to the other related channels.

Table 7 The results regarding watermarking through PSNR, SSIM, NC, and the overall score in the three separate images for different channels in the HSI model

Channel	PSNR			SSIM		
	Lena	Peppers	Baboon	Lena	Peppers	Baboon
H	14.17	22.39	20.81	0.4550	0.7419	0.8720
S	43.16	42.88	42.19	0.9814	0.9871	0.9919
I	39.37	37.54	33.76	0.9656	0.9508	0.9630
Channel	Score			NC		
	Lena	Peppers	Baboon	Lena	Peppers	Baboon
H	4.2246	6.9562	8.2422	0.3418	0.6776	0.8366
S	9.6355	9.6110	9.8033	0.9331	0.9287	0.9346
I	10.1418	10.0706	9.9972	0.9331	0.9346	0.9346

Table 8 The results regarding watermarking through PSNR, SSIM, NC, and the overall score in the three separate images for different channels in the HSV model

Channel	PSNR			SSIM		
	Lena	Peppers	Baboon	Lena	Peppers	Baboon
H	16.39	22.77	22.44	0.5722	0.7536	0.8851
S	52.22	44.37	28.52	0.9866	0.9871	0.9884
V	42.03	40.45	34.46	0.9818	0.9751	0.9705
Channel	Score			NC		
	Lena	Peppers	Baboon	Lena	Peppers	Baboon
H	4.5542	7.4484	8.5254	0.4116	0.7816	0.9004
S	10.1134	9.9729	9.4835	0.9346	0.9316	0.9346
V	10.1425	10.1459	10.0133	0.9316	0.9346	0.9346

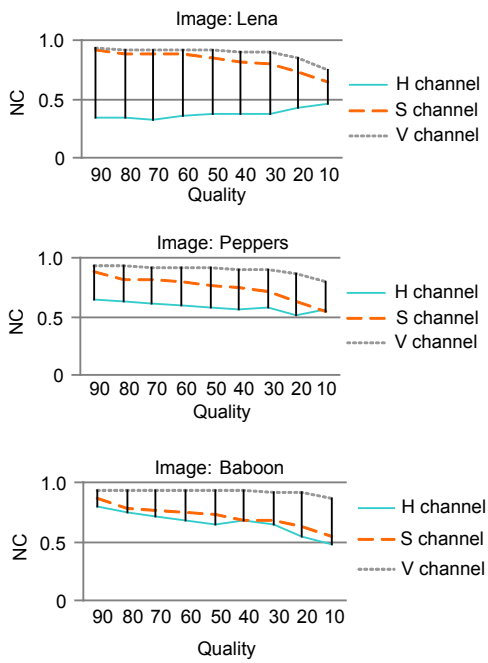

Fig. 17 Calculation of NC against JPEG compression attacks in the HSV model

The behavior of the approach in a number of channels of color models under varying watermarking intensities can now be analyzed. This is realized by changing the watermarking intensity in the span of 1 to 100, to acquire a number of important indices. Fig. 18 depicts the variation of PSNR in the I channel of the HSI model versus the corresponding variation of watermarking intensity. Fig. 19 presents the variation of SSIM in the I channel of the HSI model versus the corresponding variation of watermarking intensity, and Fig. 20 illustrates the variation of NC in the I channel of the HSI model versus the corresponding variation of watermarking intensity.

The variation of the bit error rate (BER) in the aforementioned channel of the same HSI model versus the corresponding variation of watermarking intensity is illustrated in Fig. 21.

In the sequel, Fig. 22 illustrates the variation of the score in the I channel of the HSI model versus the corresponding variation of watermarking intensity. Based upon the results in Figs. 20–21, the optimum

watermarking intensity values are taken in the span of 40–50. The results regarding the HSI model are tabulated in Table 9.

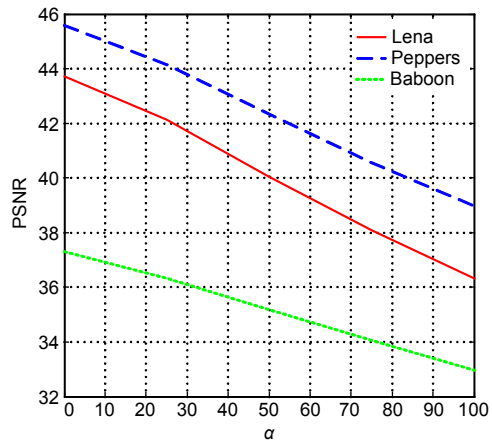

Fig. 18 Variation of PSNR in the I channel of the HSI model versus the corresponding variation of watermarking intensity

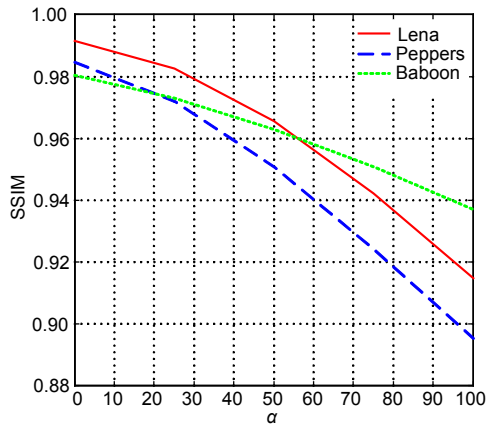

Fig. 19 Variation of SSIM in the I channel of the HSI model versus the corresponding variation of watermarking intensity

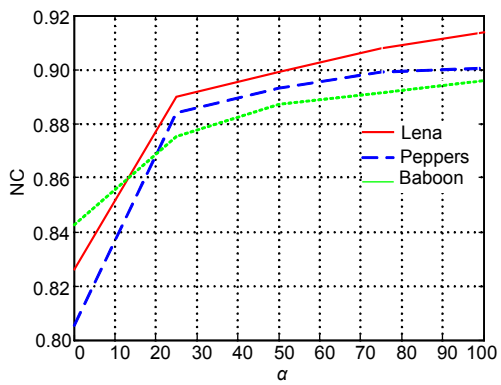

Fig. 20 Variation of NC in the I channel of the HSI model versus the corresponding variation of watermarking intensity

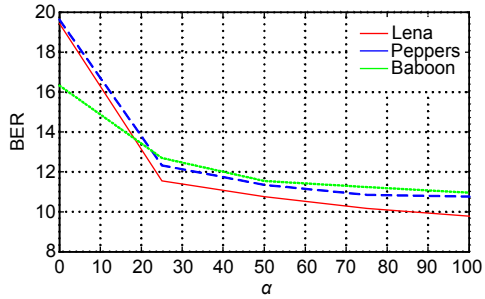

Fig. 21 Variation of BER in the I channel of the HSI model versus the corresponding variation of watermarking intensity

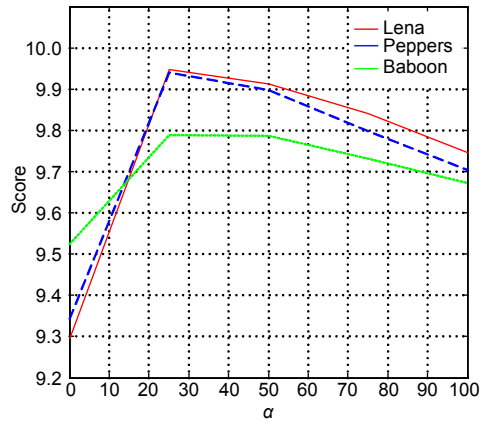

Fig. 22 Variation of the score in the I channel of the HSI model versus the corresponding variation of watermarking intensity

The results calculated through the proposed approach in line with Table 9 are illustrated in Fig. 23. Subsequently, the image histogram attacks in correspondence with Table 9 are illustrated in Figs. 24–27, where the information of the original image (Org), the watermarked image (Wtm), and the whole of the above-referenced attacks is provided. These results are useful for considering the performance of the proposed approach, as the outcomes in line with Fig. 23 indicate that the procedure of the watermarking framework behaved well.

3.1 Verification of the proposed approach

Using the proposed approach with constant watermarking intensity, the results are first acquired with a focus on NC against a set of attacks, and then compared with a number of potential benchmarks including the Tsougenis approach and the Tao approach (Table 10).

Table 9 The results of the proposed approach performance against a number of simulated attacks in the I channel regarding the model of HSI under the constant watermarking intensity (taken as 50)

Attack	NC			BER		
	Lena	Peppers	Baboon	Lena	Peppers	Baboon
Attack 1: quality JPG comp. 90	0.9302	0.9346	0.9346	8.8867	8.5938	8.5938
Attack 2: quality JPG comp. 50	0.9257	0.9346	0.9346	9.2773	8.5938	8.5938
Attack 3: median filtering 3×3	0.9316	0.9331	0.9287	8.8867	8.9844	9.2773
Attack 4: average filtering 3×3	0.9316	0.9315	0.9361	10.3516	10.2539	9.5703
Attack 5: Gaussian noise (0.001)	0.9331	0.9346	0.9346	8.6914	8.6914	8.5938
Attack 6: Salt & Peppers noise (0.001)	0.9346	0.9346	0.9331	8.5938	8.6914	8.6914
Attack 7: Salt & Peppers noise (0.01)	0.9316	0.9346	0.9331	8.8867	8.6914	8.7891
Attack 8: speckle noise (0.001)	0.9331	0.9346	0.9346	8.6914	8.6914	8.5938
Attack 9: speckle noise (0.01)	0.9302	0.9346	0.9331	8.8867	8.8867	8.7891
Attack 10: crop 1	0.8945	0.9004	0.8975	11.1328	10.8398	10.9375
Attack 11: crop 2	0.9212	0.9198	0.9138	10.0586	10.1563	11.4258
Attack 12: crop 3	0.9004	0.8915	0.8886	12.3047	13.3789	13.0859

Table 10 Comparison of the proposed approach with respect to the benchmarks against a set of attacks

Image	Approach	Salt & Peppers noise	Poisson noise	Median filter 3×3	Median filter 5×5
Lena	Proposed	0.9331	0.9316	0.9316	0.9198
	Tsougenis *et al.* (2014)	0.9149	0.9562	0.9785	0.9029
	Tao *et al.* (2014)	0.8595	0.3656	0.9528	0.8681
Peppers	Proposed	0.9346	0.9346	0.9331	0.9123
	Tsougenis *et al.* (2014)	0.9010	0.9493	0.9599	0.9053
	Tao *et al.* (2014)	0.7292	0.6585	0.8986	0.8761
Baboon	Proposed	0.9346	0.9331	0.9287	0.9167
	Tsougenis *et al.* (2014)	0.8975	0.9387	0.8806	0.8867
	Tao *et al.* (2014)	0.8093	0.4969	0.3092	0.3186

Regarding the Tsougenis approach, the key idea of the proposed moment based color image watermarking framework is first carried out in similar situations for comparison.

Regarding the Tao approach, a set of methods are efficient in the area of watermarking domains, where the idea of three-level discrete wavelet transform is carried out in similar situations for comparison. The two mentioned benchmarks are simulated through the MATLAB programing language along with the proposed approach, and the results are documented. Table 11 shows the results of NC regarding the proposed approach with respect to the benchmarks against a set of geometrical attacks.

Table 11 Comparison of the proposed approach with respect to the benchmarks against a set of geometrical attacks

Image	Approach	Crop 10%	Histogram equalization	Rotation degree
Lena	Proposed	0.9240	0.9316	0.5884
	Tsougenis'	0.9378	0.9503	0.8757
	Tao's	0.8663	0.8867	0.7532
Peppers	Proposed	0.9170	0.9272	0.6374
	Tsougenis'	0.9283	0.9698	0.8593
	Tao's	0.8679	0.8643	0.7178
Baboon	Proposed	0.9134	0.9287	0.6345
	Tsougenis'	0.9243	0.7936	0.7881
	Tao's	0.8090	0.3733	0.1812

Fig. 23 Results of the proposed approach performance against a number of simulated attacks in correspondence with Table 9

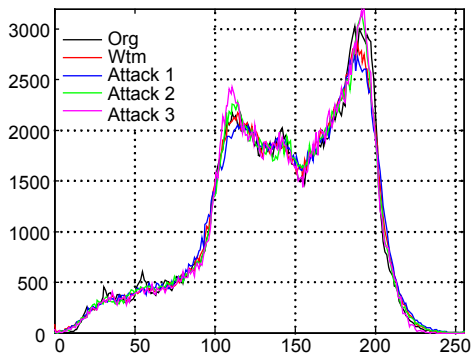

Fig. 24 The image histograms under attacks 1–3

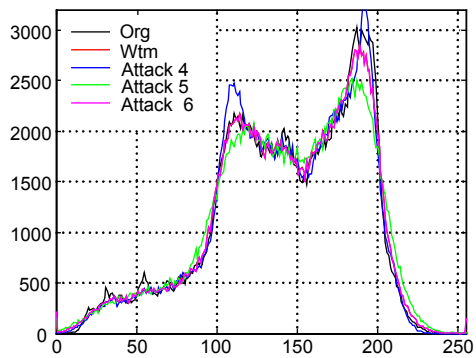

Fig. 25 The image histograms under attacks 4–6

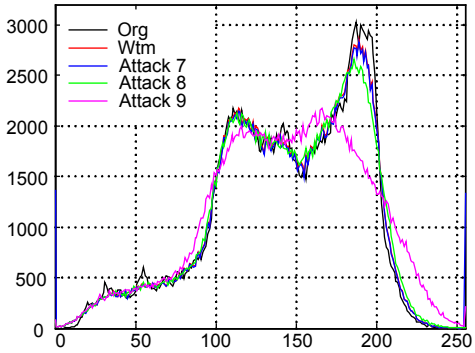

Fig. 26 The image histograms under attacks 7–9

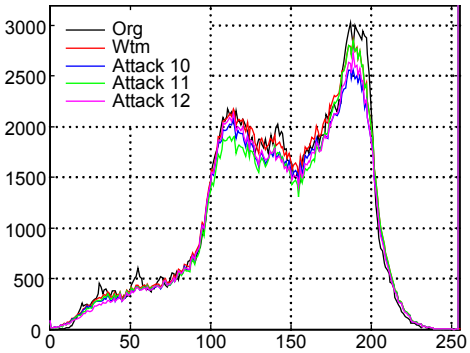

Fig. 27 The image histograms under attacks 10–12

4 Conclusions

The present research describes a new image watermarking framework through level-direction decomposition analysis. The main process of realizing the watermarking framework is investigated through contourlet embedding representation to generate a watermarked image. A number of original images are chosen to apply against a scrambling module to represent the information in disorder, while the module of the inverse of CT representation is researched to retrieve the present watermarked image. A decision making system is designed to find the best level and the corresponding direction in the level-direction decomposition transformation regarding CT embedding representation. Using several indices including the peak signal-to-noise ratio and structural similarity, the approach performance is thoroughly evaluated, while the calculation of normal correlation is considered. A set of attacks in some image colored models were carried out. Comparison with a number of benchmarks indicated that the proposed watermarking framework is efficient and the performance is coherent.

References

Abdallah, H.A., Ghazy, R.A., Kasban, H., *et al.*, 2014. Homomorphic image watermarking with a singular value decomposition algorithm. *Inform. Process. Manag.*, **50**(6):909-923. http://dx.doi.org/10.1016/j.ipm.2014.07.001

Agarwal, C., Mishra, A., Sharma, A., 2013. Gray-scale image watermarking using GA-BPN hybrid network. *J. Vis. Commun. Image Represent.*, **24**(7):1135-1146. http://dx.doi.org/10.1016/j.jvcir.2013.07.007

Agarwal, C., Mishra, A., Sharma, A., 2015. A novel gray-scale image watermarking using hybrid Fuzzy-BPN architecture. *Egypt. Inform. J.*, **16**(1):83-102. http://dx.doi.org/10.1016/j.eij.2015.01.002

Ali, M., Ahn, C.W., 2015. Comments on "Optimized gray-scale image watermarking using DWT-SVD and firefly algorithm". *Exp. Syst. Appl.*, **42**(5):2392-2394. http://dx.doi.org/10.1016/j.eswa.2014.10.045

Ali, M., Ahn, C.W., Pant, M., *et al.*, 2015. An image watermarking scheme in wavelet domain with optimized compensation of singular value decomposition via artificial bee colony. *Inform. Sci.*, **301**:44-60. http://dx.doi.org/10.1016/j.ins.2014.12.042

Al-Otum, H.M., 2014. Semi-fragile watermarking for gray-scale image authentication and tamper detection based on an adjusted expanded-bit multiscale quantization-based technique. *J. Vis. Commun. Image Represent.*, **25**(5): 1064-1081. http://dx.doi.org/10.1016/j.jvcir.2013.12.017

Cai, N., Zhu, N.N., Weng, S.W., *et al.*, 2015. Difference angle quantization index modulation scheme for image watermarking. *Signal Process. Image Commun.*, **34**:52-60. http://dx.doi.org/10.1016/j.image.2015.03.010

Chen, B.J., Coatrieux, G., Chen, G., *et al.*, 2014. Full 4-D quaternion discrete Fourier transform based watermarking for color images. *Dig. Signal Process.*, **28**:106-119. http://dx.doi.org/10.1016/j.dsp.2014.02.010

Chen, H.Y., Zhu, Y.S., 2012. A robust watermarking algorithm based on QR factorization and DCT using quantization index modulation technique. *J. Zhejiang Univ.-Sci. C (Comput. & Electron.)*, **13**(8):573-584. http://dx.doi.org/10.1631/jzus.C1100338

Dadkhah, S., Manaf, A.A., Hori, Y., *et al.*, 2014. An effective SVD-based image tampering detection and self-recovery using active watermarking. *Signal Process. Image Commun.*, **29**(10):1197-1210. http://dx.doi.org/10.1016/j.image.2014.09.001

Dinh, D.L., Lim, M.J., Thang, N.D., *et al.*, 2014. Real-time 3D human pose recovery from a single depth image using principal direction analysis. *Appl. Intell.*, **41**(2):473-486. http://dx.doi.org/10.1007/s10489-014-0535-z

Do, M.N., Vetterli, M., 2001. Pyramidal directional filter banks and curvelets. Proc. Int. Conf. on Image Processing. http://dx.doi.org/10.1109/ICIP.2001.958075

Guo, J.M., Prasetyo, H., 2014. False-positive-free SVD-based image watermarking. *J. Vis. Commun. Image Represent.*, **25**(5):1149-1163. http://dx.doi.org/10.1016/j.jvcir.2014.03.012

Lei, B.Y., Tan, E.L., Chen, S.P., *et al*., 2014. Reversible watermarking scheme for medical image based on differential evolution. *Exp. Syst. Appl.*, **41**(7):3178-3188. http://dx.doi.org/10.1016/j.eswa.2013.11.019

Makbol, N.M., Khoo, B.E., 2014. A new robust and secure digital image watermarking scheme based on the integer wavelet transform and singular value decomposition. *Dig. Signal Process.*, **33**:134-147. http://dx.doi.org/10.1016/j.dsp.2014.06.012

Mishra, A., Agarwal, C., Sharma, A., *et al*., 2014. Optimized gray-scale image watermarking using DWT–SVD and Firefly Algorithm. *Exp. Syst. Appl.*, **41**(17):7858-7867. http://dx.doi.org/10.1016/j.eswa.2014.06.011

Niu, P.P., Wang, X.Y., Yang, Y.P., *et al*., 2011. A novel color image watermarking scheme in nonsampled contourlet-domain. *Exp. Syst. Appl.*, **38**(3):2081-2098. http://dx.doi.org/10.1016/j.eswa.2010.07.147

Ouyang, J., Coatrieux, G., Chen, B., *et al.*, 2015. Color image watermarking based on quaternion Fourier transform and improved uniform log-polar mapping. *Comput. Electr. Eng.*, **38**(3):2081-2098. http://dx.doi.org/10.1016/j.eswa.2010.07.147

Qi, M., Li, B.Z., Sun, H.F., 2015. Image watermarking using polar harmonic transform with parameters in *SL* (2, R). *Signal Process. Image Commun.*, **31**:161-173. http://dx.doi.org/10.1016/j.image.2014.12.009

Shao, Z.H., Duan, Y.P., Coatrieux, G., *et al*., 2015. Combining double random phase encoding for color image watermarking in quaternion gyrator domain. *Opt. Commun.*, **343**:56-65. http://dx.doi.org/10.1016/j.optcom.2015.01.002

Su, Q.T., Niu, Y.G., Wang, G., *et al*., 2014. Color image blind watermarking scheme based on QR decomposition. *Signal Process.*, **94**:219-235. http://dx.doi.org/10.1016/j.sigpro.2013.06.025

Tao, H., Li, C.M., Zain, J.M., *et al*., 2014. Robust image watermarking theories and techniques: a review. *J. Appl. Res. Technol.*, **12**(1):122-138. http://dx.doi.org/10.1016/S1665-6423(14)71612-8

Tsougenis, E.D., Papakostas, G.A., Koulouriotis, D.E., *et al*., 2013. Towards adaptivity of image watermarking in polar harmonic transforms domain. *Opt. Laser Technol.*, **54**:84-97. http://dx.doi.org/10.1016/j.optlastec.2013.05.004

Tsougenis, E.D., Papakostas, G.A., Koulouriotis, D.E., *et al*., 2014. Adaptive color image watermarking by the use of quaternion image moments. *Exp. Syst. Appl.*, **41**(14): 6408-6418. http://dx.doi.org/10.1016/j.eswa.2014.04.021

Wang, H., Ho, A.T.S., Li, S.J., 2014. A novel image restoration scheme based on structured side information and its application to image watermarking. *Signal Process. Image Commun.*, **29**(7):773-787. http://dx.doi.org/10.1016/j.image.2014.05.001

Wang, X.Y., Niu, P.P., Yang, H.Y., *et al*., 2014. A new robust color image watermarking using local quaternion exponent moments. *Inform. Sci.*, **277**:731-754. http://dx.doi.org/10.1016/j.ins.2014.02.158

Yadav, A.K., Vashisth, S., Singh, H., *et al.*, 2015. A phase-image watermarking scheme in gyrator domain using Devil's vortex Fresnel lens as a phase mask. *Opt. Commun.*, **344**(1):172-180. http://dx.doi.org/10.1016/j.optcom.2015.01.019

Yang, H.Y., Zhang, Y., Wang, P., *et al.*, 2014. A geometric correction based robust color image watermarking scheme using quaternion exponent moments. *Optik Int. J. Light Electron Opt.*, **125**(16):4456-4469. http://dx.doi.org/10.1016/j.ijleo.2014.02.028

Yu, M., Wang, J., Jiang, G.Y., *et al*., 2015. New fragile watermarking method for stereo image authentication with localization and recovery. *AEU Int. J. Electron. Commun.*, **69**(1):361-370. http://dx.doi.org/10.1016/j.aeue.2014.10.006

Zhan, Y.Z., Li, Y.T., Wang, X.Y., *et al*., 2014. A blind watermarking algorithm for 3D mesh models based on vertex curvature. *J. Zhejiang Univ.-Sci. C (Comput. & Electron.)* **15**(5):351-362. http://dx.doi.org/10.1631/jzus.C1300306